J. Fluid Mech. (1984), *vol.* 139, *pp.* 461–471
Printed in Great Britain

The transition from roll to square-cell solutions in Rayleigh–Bénard convection

By D. R. JENKINS AND M. R. E. PROCTOR
Department of Applied Mathematics and Theoretical Physics,
Silver Street, Cambridge CB3 9EW, England

(Received 11 July 1983)

We consider three-dimensional finite-amplitude thermal convection in a fluid layer with boundaries of finite conductivity. Busse & Riahi (1980) and Proctor (1981) showed that the preferred planform of convection in such a system is a square-cell tesselation provided that the boundaries are much poorer conductors than the fluid, in contrast to the roll solutions which are obtained for perfectly conducting boundaries. We determine here the conductivity of the boundaries at which the preferred planform changes from roll to square-cell type. We show that, for low-Prandtl-number fluids (e.g. mercury), square-cell solutions are realized only when the boundaries are almost insulating; while, for high-Prandtl-number fluids (e.g. silicone oils), square-cell solutions are stable when the boundaries have conductivity comparable to that of the fluid.

1. Introduction

The study of thermal convection in a horizontal layer of fluid heated from below has many physical applications, notably in astrophysics and geophysics, as well as industrial processes. Typically this phenomenon is modelled by considering the boundaries of the fluid as perfect conductors of heat. One can approximate these conditions in the laboratory but they are not always relevant in actual applications. The extent to which the departure from this ideal affects the nature of the solutions is therefore of interest. Jeffreys (1926) investigated the linear stability of a layer whose boundaries were perfect insulators, but an error in the velocity boundary conditions led him to incorrect conclusions regarding the onset of convection. Sparrow, Goldstein & Jonsson (1964) and Hurle, Jakeman & Pike (1967) carried out linear stability analyses of the problem of convection between layers that are much poorer conductors than the fluid. These authors found that the horizontal wavenumber of the most-unstable convection mode tends to zero as the ratio ζ of the thermal conductivity of the boundary to that of the fluid approaches zero. Thus the horizontal scale of convection in this case is much larger than the depth of the fluid. Chapman & Proctor (1980) have used the disparity of scales to develop an expansion scheme for the nonlinear equations in terms of the small horizontal wavenumber, for two-dimensional motion. The same method was employed by Proctor (1981) to consider three-dimensional convection at small values of ζ, and Prandtl numbers of order unity, with the depths of the boundaries being of the same order as the depth of the fluid. He found that, for sufficiently small values of ζ, the preferred planform of convection is a square cell. A similar result was obtained by Busse & Riahi (1980) using the small-amplitude perturbation approach developed by Malkus & Veronis

(1958) and Schluter, Lortz & Busse (1965); Busse & Riahi showed also that the square-cell convection pattern led to a higher value of convective heat transport than either two-dimensional rolls or three-dimensional hexagonal cells.

In the present paper we use a small-amplitude expansion procedure of similar type to determine the value of ζ at which the preferred planform of convection changes from square cells (which occur for sufficiently small ζ) to roll cells (which occur for the case of infinite ζ). The nonlinear stability problem is reduced to a sequence of inhomogeneous boundary-value problems. The solution of this sequence of problems is continued until a 'solvability condition' is obtained which yields evolution equations describing the nonlinear interaction of rolls and squares for a given value of ζ. (Hexagonal solutions are not considered, as they are ruled out by the result of Busse & Riahi (1980) as well as those of Proctor (1981).) These equations may be solved to find the stable steady planform at finite amplitude. A similar method has been used for the investigation of convection in a porous medium by Riahi (1983).

In §2 the problem is formulated. A summary of the linear stability theory for the problem is presented in §3 and the eigenfunctions as well as the eigenvalues of the linear problem are determined. The expansion procedure applied to the nonlinear equations is presented in §4, which results in a set of nonlinear o.d.e.s for the amplitude of the horizontal modes. The results of this analysis are given in §5 and are discussed in §6. The main result of the paper is that the conductivity ratio at which the changeover occurs depends strongly on the Prandtl number σ. For large σ the transition occurs when the conductivities of fluid and boundary are similar, while for small σ the critical value $\zeta_c \sim \sigma^4$, except when the solid slabs are infinitely thick, in which case $\zeta_c \sim \sigma^3$ (see figure 3).

2. Formulation

We consider a layer of Boussinesq fluid of depth d located between solid slabs of depth $\frac{1}{2}\lambda d$, where λ is of order unity. The thermal conductivity of the fluid is k and of the slabs is k_1; the respective thermal diffusivities κ and κ_1 are obtained by dividing the conductivity by ρc_p, where ρ is the density and c_p the specific heat of the appropriate region. All of k, k_1, κ and κ_1 are assumed to be constant. Cartesian coordinates are chosen with the origin at the midpoint of the layer. Gravity $\boldsymbol{g}$ is perpendicular to the boundaries of the fluid; the fluid has velocity $\boldsymbol{u}$, pressure p and kinematic viscosity ν. The temperature T is fixed at the outer surfaces of the bounding slabs, so that the overall temperature difference is ΔT. Thus when $\boldsymbol{u} = 0$, the temperature gradient in the fluid is

$$-q \equiv \frac{\Delta T}{d(1+\lambda/\zeta)}, \tag{2.1a}$$

and

$$T = T_0 - qz \quad (|z| \leqslant \tfrac{1}{2}d), \tag{2.1b}$$

$$T = T_0 \mp \tfrac{1}{2}qd(1-\zeta^{-1}) - q\zeta^{-1}z \quad \begin{cases} (\frac{1}{2}d \leqslant z \leqslant \frac{1}{2}(1+\lambda)\,d), \\ (-\frac{1}{2}d \geqslant z \geqslant -\frac{1}{2}(1+\lambda)\,d), \end{cases} \tag{2.1c}$$

where $\zeta = k_1/k$ and T_0 is a reference temperature at which the fluid density is ρ_0. If the temperature perturbation due to any fluid motion is $\theta(\boldsymbol{x}, t)$ in the fluid and is $\tilde{\theta}(\boldsymbol{x}, t)$ in the solid, and α is the coefficient of thermal expansion, then the non-dimensional

equations of motion and heat are

$$\frac{1}{\sigma}\left[\frac{\partial \boldsymbol{u}}{\partial t}+\boldsymbol{u}\cdot\nabla\boldsymbol{u}\right]=-\nabla p+R\theta\hat{\boldsymbol{z}}+\nabla^2\boldsymbol{u}, \tag{2.2a}$$

$$\frac{\partial\theta}{\partial t}+\boldsymbol{u}\cdot\nabla\theta=\boldsymbol{u}\cdot\hat{\boldsymbol{z}}+\nabla^2\theta, \tag{2.2b}$$

$$\nabla\cdot\boldsymbol{u}=0, \tag{2.2c}$$

in the fluid, and

$$\frac{\partial\tilde{\theta}}{\partial t}=\frac{\kappa_1}{\kappa}\nabla^2\tilde{\theta} \tag{2.3}$$

in the bounding slabs. In (2.2) and (2.3), $\hat{\boldsymbol{z}}$ is the unit vector antiparallel to $\boldsymbol{g}$, $|\boldsymbol{u}|$ is scaled with κ/d, p with $\rho_0\nu\kappa d^2$, time t with d^2/κ, lengths with d and θ, $\tilde{\theta}$ with qd. The dimensionless parameters are $\sigma=\nu/\kappa$, the Prandtl number of the fluid and R, the Rayleigh number, defined by

$$R=\frac{|\boldsymbol{g}|\,\alpha q d^4}{\kappa\nu}. \tag{2.4}$$

The velocity vanishes on the boundaries $z=\pm\frac{1}{2}$, and the temperature boundary conditions are

$$\tilde{\theta}=0 \quad (z=\pm\tfrac{1}{2}(1+\lambda)), \tag{2.5}$$

$$\theta=\tilde{\theta} \quad (z=\pm\tfrac{1}{2}), \tag{2.6}$$

$$\mathrm{D}\theta=\zeta\,\mathrm{D}\tilde{\theta} \quad (z=\pm\tfrac{1}{2}), \tag{2.7}$$

where D represents $\partial/\partial z$. We seek small- (but finite-)amplitude velocity and temperature fields that are periodic in x and y, thus giving the tesselated cellular structure often observed in experiments, and determine the preferred planform.

3. Linear stability theory

In the linear problem the velocity $\boldsymbol{u}$ is poloidal and may be written in terms of the scalar field $\phi(\boldsymbol{x},t)$ as

$$\boldsymbol{u}=\nabla\times\nabla\times(\phi\hat{\boldsymbol{z}}). \tag{3.1}$$

Substituting (3.1) into (2.2) and ignoring nonlinear terms in the resulting equations for ϕ, θ and $\tilde{\theta}$ leads to a system separable in x, y and t which describes the evolution of small disturbances. It is easily shown that if $\boldsymbol{u},\theta,\tilde{\theta}\propto \mathrm{e}^{st}$ then s must be real, and so the boundary between growing and decaying solutions is given by $s=0$. Writing $\phi=f(x,y)\,h(z)$, $\theta=f(x,y)\,g(z)$ and $\tilde{\theta}=f(x,y)\,\tilde{g}(z)$, where $\nabla_{\mathrm{H}}^2 f=-\alpha^2 f$, the equations for steady fields become

$$(\mathrm{D}^2-\alpha^2)\,\tilde{g}=0, \tag{3.2a}$$

$$0=Rg-(\mathrm{D}^2-\alpha^2)^2 h, \tag{3.2b}$$

$$0=\alpha^2 h+(\mathrm{D}^2-\alpha^2)\,g. \tag{3.2c}$$

which are to be solved subject to the appropriate boundary conditions derived from (2.5)–(2.7) (see also (4.4) below). The parameter α is thus a horizontal wavenumber and should not be confused with the coefficient of thermal expansion defined in §2. The critical value of $R(=R_0)$ for linear instability is thus a function of ζ, λ and α^2 determined as an eigenvalue of (3.2). The minimum value of R_0 as a function of α with ζ and λ both fixed has been determined by Proctor (1981) and the results are shown in figure 1 for a range of values of ζ, with $\lambda=1$. For the purposes of the present

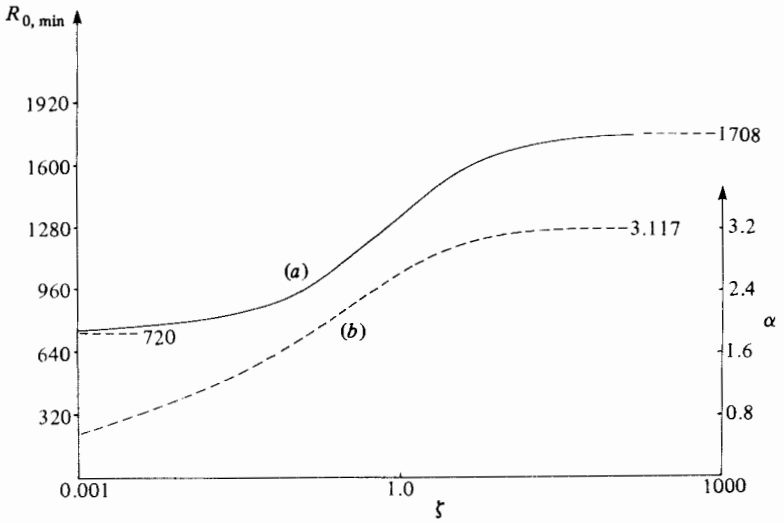

FIGURE 1. Graphs of (*a*) critical Rayleigh number $R_{0,\min}$ and (*b*) critical wavenumber α_c as functions of ζ for $\lambda = 1$ (after Proctor 1981). Note that Proctor uses a different scaling for the layer depth.

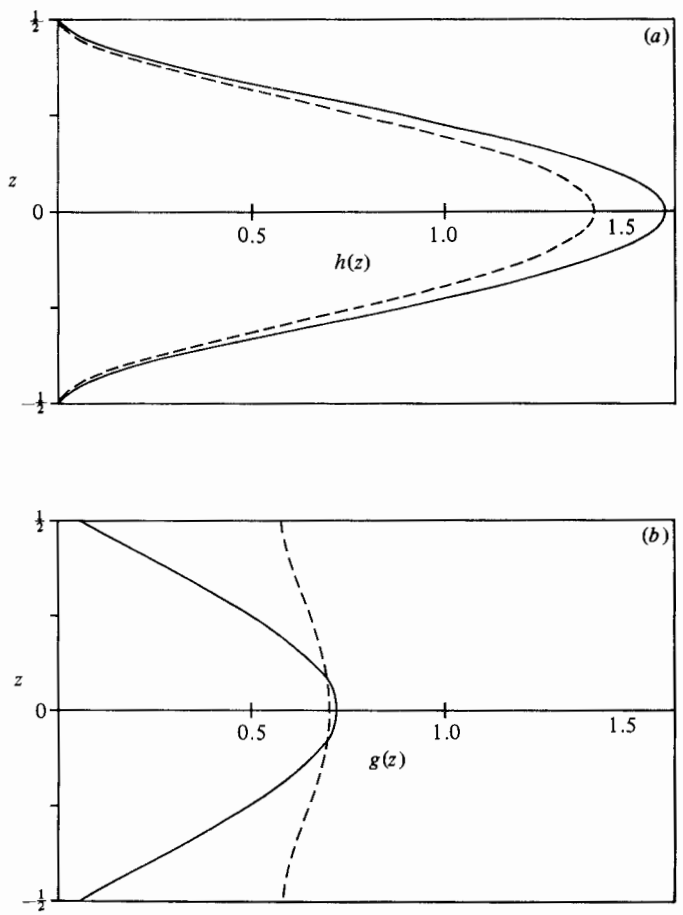

FIGURE 2. Graphs of the eigenfunctions for the vertical dependence of (*a*) velocity $h(z)$ and (*b*) fluid temperature $g(z)$ for boundaries that are poorly conducting ($\zeta = 0.1$, dashed line) and highly conducting ($\zeta = 10$, solid line).

analysis it is convenient also to determine the eigenfunctions $g(z)$ $h(z)$, and $\tilde{g}(z)$ accurately. This has been achieved using a finite-difference method which determines both the eigenvalues and the eigenfunctions of the system (3.2). These calculations have been used to verify the results of Proctor (1981), whereby the graph of figure 1 was reproduced. Figure 2 shows typical eigenfunctions, suitably normalized, of the system (3.2) for different values of ζ.

4. Nonlinear small-amplitude theory

Returning to the original equations (2.2) we expand R, $\boldsymbol{u}$, θ, $\tilde{\theta}$ and p in powers of a small parameter ϵ as

$$R = R_0 + \epsilon^2 R_2 + \ldots, \tag{4.1a}$$

$$\boldsymbol{u} = \epsilon \boldsymbol{u}_1 + \epsilon^2 \boldsymbol{u}_2 + \epsilon^3 \boldsymbol{u}_3 + \ldots, \tag{4.1b}$$

$$\theta = \epsilon\theta_1 + \epsilon^2\theta_2 + \epsilon^3\theta_3 + \ldots, \tag{4.1c}$$

$$\tilde{\theta} = \epsilon\tilde{\theta}_1 + \epsilon^2\tilde{\theta}_2 + \epsilon^3\tilde{\theta}_3 + \ldots, \tag{4.1d}$$

$$p = \epsilon p_1 + \epsilon^2 p_2 + \epsilon^3 p_3 + \ldots, \tag{4.1e}$$

and scale the time t as

$$\frac{\partial}{\partial t} = \epsilon^2 \frac{\partial}{\partial \tau}. \tag{4.2}$$

There is no term ϵR_1 in (4.1a) since the physics of the problem does not depend on the sign of $\boldsymbol{u}$; the scaling of time is the usual one for weakly nonlinear convection (see e.g. Malkus & Veronis 1958). We then substitute (4.1) into (2.2) and the boundary conditions (2.5)–(2.7) and attempt to solve the sequence of problems that emerges. At leading order, this yields the linear problem discussed in §3, with the solution

$$\boldsymbol{u}_1 = \boldsymbol{\nabla} \times \boldsymbol{\nabla} \times (\phi_1 \hat{\boldsymbol{z}}), \tag{4.3a}$$

$$\phi_1 = f(x, y, \tau)\, h(z), \tag{4.3b}$$

$$\theta_1 = f(x, y, \tau)\, g(z), \tag{4.3c}$$

$$\tilde{\theta}_1 = f(x, y, \tau)\, \tilde{g}(z), \tag{4.3d}$$

where

$$\nabla_{\mathrm{H}}^2 f = -\alpha^2 f, \tag{4.4}$$

$$\tilde{g}(z) = \theta_1(\pm\tfrac{1}{2}) \frac{\sinh\left[\alpha(\tfrac{1}{2}(1+\lambda) \mp z)\right]}{\sinh\left[\tfrac{1}{2}\alpha\lambda\right]} \quad \begin{cases} (\tfrac{1}{2} \leqslant z \leqslant \tfrac{1}{2}(1+\lambda)), \\ (-\tfrac{1}{2} \leqslant z \leqslant \tfrac{1}{2}(1+\lambda)), \end{cases} \tag{4.5}$$

and

$$R_0 = R_{0,\min}, \tag{4.6}$$

where $R_{0,\min}$ is the minimum value of R_0 as a function of α, and occurs at $\alpha = \alpha_{\mathrm{c}}$.

In order to determine the planform of convection occurring at values of R slightly above R_0 it is necessary to determine the nature of the evolution of the function f with time τ. To do this, we suppose that f takes the form

$$f = A(\tau)\cos\alpha_{\mathrm{c}} x + B(\tau)\cos\alpha_{\mathrm{c}} y, \tag{4.7}$$

and look for the limiting behaviour of A and B. The next order in ϵ yields the equations

$$\frac{1}{\sigma}\boldsymbol{u}_1\cdot\boldsymbol{\nabla}\boldsymbol{u}_1 = -\boldsymbol{\nabla}p_2 + R_0\theta_2\hat{\boldsymbol{z}} + \nabla^2\boldsymbol{u}_2, \tag{4.8a}$$

$$\boldsymbol{u}_1\cdot\boldsymbol{\nabla}\theta_1 = \boldsymbol{u}_2\cdot\hat{\boldsymbol{z}} + \nabla^2\theta_2, \tag{4.8b}$$

$$0 = \nabla^2\tilde{\theta}_2, \tag{4.8c}$$

$$0 = \boldsymbol{\nabla}\cdot\boldsymbol{u}_2, \tag{4.8d}$$

and the boundary conditions

$$\boldsymbol{u}_2 = 0, \quad \theta_2 = \tilde{\theta}_2, \quad \mathrm{D}\theta_2 = \zeta\,\mathrm{D}\tilde{\theta}_2 \quad (z = \pm\tfrac{1}{2}), \tag{4.9a}$$

$$\tilde{\theta}_2 = 0 \quad (z = \pm\tfrac{1}{2}(1+\lambda)). \tag{4.9b}$$

In order to solve the equations (4.8), we first take $\hat{\boldsymbol{z}}\cdot\boldsymbol{\nabla}\times\boldsymbol{\nabla}\times$ of the first of these equations, which yields

$$-\frac{1}{\sigma}\hat{\boldsymbol{z}}\cdot\boldsymbol{\nabla}\times\boldsymbol{\nabla}\times(\boldsymbol{u}_1\cdot\boldsymbol{\nabla}\boldsymbol{u}_1) = \nabla^4 w_2 + R_0\nabla_{\mathrm{H}}^2\theta_2, \tag{4.10}$$

where $w_2 = \boldsymbol{u}_2\cdot\hat{\boldsymbol{z}}$, and solve (4.10) along with the remaining equations in (4.8) involving θ_2 and $\tilde{\theta}_2$. The terms on the left-hand sides of (4.8) and (4.10) require that w_2, θ_2 and $\tilde{\theta}_2$ take the form

$$\chi = (A^2+B^2)\chi^{(1)}(z) + A^2\cos 2\alpha x\chi^{(2)}(z) + B^2\cos 2\alpha y\chi^{(3)}(z) + AB\cos\alpha x\cos\alpha y\chi^{(4)}(z), \tag{4.11}$$

where the symbol χ stands for w_2, θ_2 and $\tilde{\theta}_2$ respectively and the $\chi^{(i)}(z)$ satisfy a set of linear o.d.e.s determined by substitution of (4.11) into (4.8)–(4.10). Notably, we find that $w_2^{(1)} = 0$ and $\chi^{(2)} = \chi^{(3)}$ due to the symmetry of the problem. The remaining set of o.d.e.s may be solved numerically on the same finite-difference grid as that used for $g(z)$, $h(z)$ and $\tilde{g}(z)$. Also, it may be shown that $\hat{\boldsymbol{z}}\cdot\boldsymbol{\nabla}\times(\boldsymbol{u}_1\cdot\boldsymbol{\nabla}\boldsymbol{u}_1) = 0$ (Schluter *et al.* 1965), so that we may write $\boldsymbol{u}_2$ as

$$\boldsymbol{u}_2 = \boldsymbol{\nabla}\times\boldsymbol{\nabla}\times(\phi_2\hat{\boldsymbol{z}}) = (\phi_{2xz}, \phi_{2yz}, -\nabla_{\mathrm{H}}^2\phi_2). \tag{4.12}$$

Thus ϕ_2 may be determined from the form for w_2 and then it is possible to determine the x- and y-components of $\boldsymbol{u}_2$ (namely u_2 and v_2):

$$u_2 = -\frac{A^2}{2\alpha}\sin 2\alpha x\,\mathrm{D}w_2^{(2)} - \frac{AB}{2\alpha}\sin\alpha x\cos\alpha y\,\mathrm{D}w_2^{(4)}, \tag{4.13a}$$

$$v_2 = -\frac{B^2}{2\alpha}\sin 2\alpha y\,\mathrm{D}w_2^{(2)} - \frac{AB}{2\alpha}\cos\alpha x\sin\alpha y\,\mathrm{D}w_2^{(4)}. \tag{4.13b}$$

Finally, taking $O(\epsilon^3)$ terms in (2.2) yields

$$\frac{1}{\sigma}\left[\frac{\partial\boldsymbol{u}_1}{\partial\tau} + \boldsymbol{u}_1\cdot\boldsymbol{\nabla}\boldsymbol{u}_2 + \boldsymbol{u}_2\cdot\boldsymbol{\nabla}\boldsymbol{u}_1\right] = -\boldsymbol{\nabla}p_3 + R_2\theta_1\hat{\boldsymbol{z}} + \nabla^2\boldsymbol{u}_3 + R_0\theta_3\hat{\boldsymbol{z}}, \tag{4.14a}$$

$$\frac{\partial\theta_1}{\partial\tau} + (\boldsymbol{u}_1\cdot\boldsymbol{\nabla}\theta_2 + \boldsymbol{u}_2\cdot\boldsymbol{\nabla}\theta_1) = \boldsymbol{u}_3\cdot\hat{\boldsymbol{z}} + \nabla^2\theta_3, \tag{4.14b}$$

$$\frac{\partial\tilde{\theta}_1}{\partial\tau} = \frac{\kappa_1}{\kappa}\nabla^2\tilde{\theta}_3, \tag{4.14c}$$

$$0 = \boldsymbol{\nabla}\cdot\boldsymbol{u}_3, \tag{4.14d}$$

with the boundary conditions

$$\boldsymbol{u}_3 = 0, \quad \theta_3 = \tilde{\theta}_3, \quad \mathrm{D}\theta_3 = \zeta \mathrm{D}\tilde{\theta}_3 \quad (z = \pm\tfrac{1}{2}), \tag{4.15a}$$

$$\tilde{\theta}_3 = 0 \quad (z = \pm\tfrac{1}{2}(1+\lambda)). \tag{4.15b}$$

We see that (4.14*a–d*) include the time derivatives of $\boldsymbol{u}_1$, θ_1 and $\tilde{\theta}_1$, and so should allow determination of the nature of the time variation of the function f. In fact, (4.14) and (4.15) constitute an inhomogeneous boundary-value problem, which has a solution if and only if the following 'solvability condition' holds for all $\boldsymbol{u}^*$, θ^* and f^* that are solutions of the homogeneous linear problem:

$$\frac{1}{\sigma}\left\langle \boldsymbol{u}^* \cdot \left[\frac{\partial \boldsymbol{u}_1}{\partial \tau} + \boldsymbol{u}_1 \cdot \nabla \boldsymbol{u}_2 + \boldsymbol{u}_2 \cdot \nabla \boldsymbol{u}_1\right]\right\rangle - R_2\langle w^*\theta_1\rangle + R_0\left\langle \theta^*\left[\frac{\partial \theta_1}{\partial \tau} + \boldsymbol{u}_1 \cdot \nabla\theta_2 + \boldsymbol{u}_2 \cdot \nabla\theta_1\right]\right\rangle$$

$$= R_0 \zeta \frac{\kappa}{\kappa_1} g(\tfrac{1}{2})^2 \frac{[\alpha\lambda - \sinh\alpha\lambda]}{2\alpha \sinh^2(\frac{1}{2}\alpha\lambda)}\left\{f^* \frac{\partial f}{\partial \tau}\right\}, \tag{4.16}$$

where $\{\ldots\}$ denotes a horizontal average and $\langle\ldots\rangle \equiv \int_{-\frac{1}{2}}^{\frac{1}{2}} \mathrm{d}z\{\ldots\}$. The term on the right-hand side of (4.16) was obtained by writing $\tilde{\theta}_3$ as

$$\tilde{\theta}_3 = \frac{\partial f}{\partial \tau} L(z), \tag{4.17}$$

and substituting into (4.14*c*).

If we write $\boldsymbol{u}_1$ as $\boldsymbol{u}_1^{(1)} + \boldsymbol{u}_1^{(2)}$, where

$$\boldsymbol{u}_1^{(i)} = \nabla \times \nabla \times (\phi_1^{(i)} \hat{\boldsymbol{z}}) \quad (i = 1, 2), \tag{4.18}$$

and

$$\phi_1^{(1)} = A(\tau)\cos\alpha x\, h(z), \tag{4.19a}$$

$$\phi_1^{(2)} = B(\tau)\cos\alpha y\, h(z), \tag{4.19b}$$

and similarly define $\theta_1^{(1)}$ and $\theta_1^{(2)}$, then each of these horizontal modes is a solution of the homogeneous problem. Hence we may apply the solvability condition (4.16) with $\boldsymbol{u}^*, \theta^*$ replaced by $\boldsymbol{u}_1^{(i)}, \theta_1^{(i)}$, $i = 1, 2$, to yield the following two differential equations for A and B:

$$D^2 \frac{\mathrm{d}A}{\mathrm{d}\tau} = R_2 A - E^2 A^3 - F^2 A B^2, \tag{4.20}$$

$$D^2 \frac{\mathrm{d}B}{\mathrm{d}\tau} = R_2 B - E^2 B^3 - F^2 A^2 B, \tag{4.21}$$

where the positive quantities D^2, E^2 and F^2 may be calculated numerically as integrals of complicated expressions involving the z-dependences of w_1, w_2 etc. The stable solutions of (4.20) and (4.21) depend on the relative magnitudes of E^2 and F^2. If $E^2 > F^2$ then the stable solutions are

$$|A| = |B| = \left(\frac{R_2}{E^2 + F^2}\right)^{\frac{1}{2}}, \tag{4.22}$$

which corresponds to a square planform. If $E^2 < F^2$ the stable solutions are

$$A = 0, \quad |B| = \left(\frac{R_2}{E^2}\right)^{\frac{1}{2}}, \tag{4.23a}$$

or

$$B = 0, \quad |A| = \left(\frac{R_2}{E^2}\right)^{\frac{1}{2}}, \tag{4.23b}$$

which correspond to roll solutions.

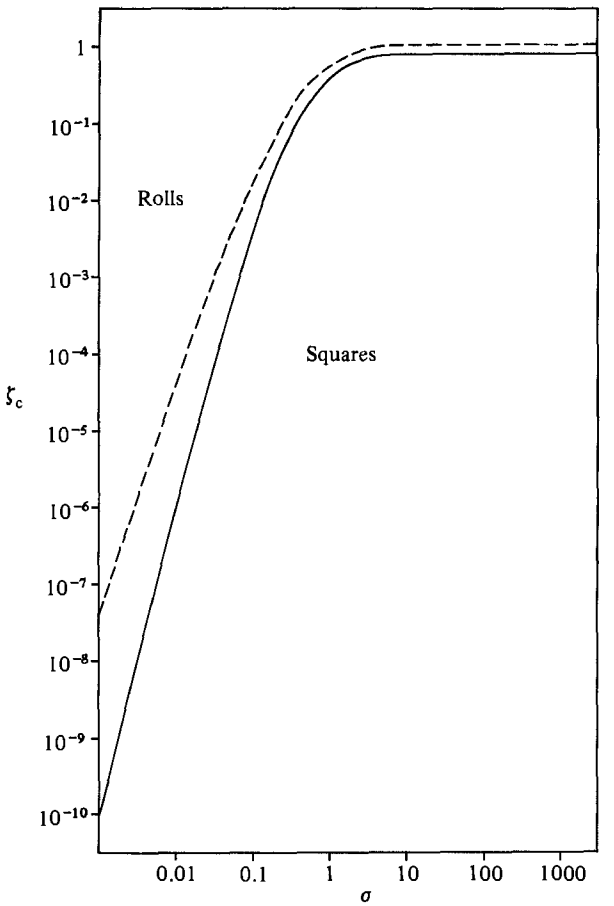

FIGURE 3. Graph of ζ_c as a function of σ for $\lambda = 1$ (solid line) and $\lambda \to \infty$ (dashed line). The stable planform is rolls for the region above each curve and square cells below. Note that the singular case $\lambda \to \infty$ obeys a different power law ($\zeta_c \sim \sigma^3$) for small σ.

Thus it is necessary to evaluate the coefficients E^2 and F^2 as a function of the parameters ζ, λ and σ. In particular, we desire to fix λ and σ, then determine the value of ζ at which $E^2 = F^2$, where the stable planform changes from roll solutions to squares.

5. Results

The interval $-\frac{1}{2} \leqslant z \leqslant \frac{1}{2}$ was divided into a finite-difference grid and the linear eigenvalue problem of §3 was solved numerically using the Method of Inverse Iteration and then the set of linear o.d.e.s arising from equations (4.8)–(4.11) was also solved using a NAG library finite-difference routine. This procedure enabled evaluation of the coefficients E^2 and F^2 for specified values of ζ, λ and σ. It was then possible to determine the value of ζ at which E^2 and F^2 are equal for particular values of λ and σ. This value (ζ_c, say) is the ratio of conductivities at which the planform of the convection changes from roll solutions ($\zeta > \zeta_c$) to square-cell solutions ($\zeta < \zeta_c$). Although it is not possible to determine ζ_c analytically, except asymptotically for small σ (see below), it may be shown, using the analysis of Proctor (1981), that the

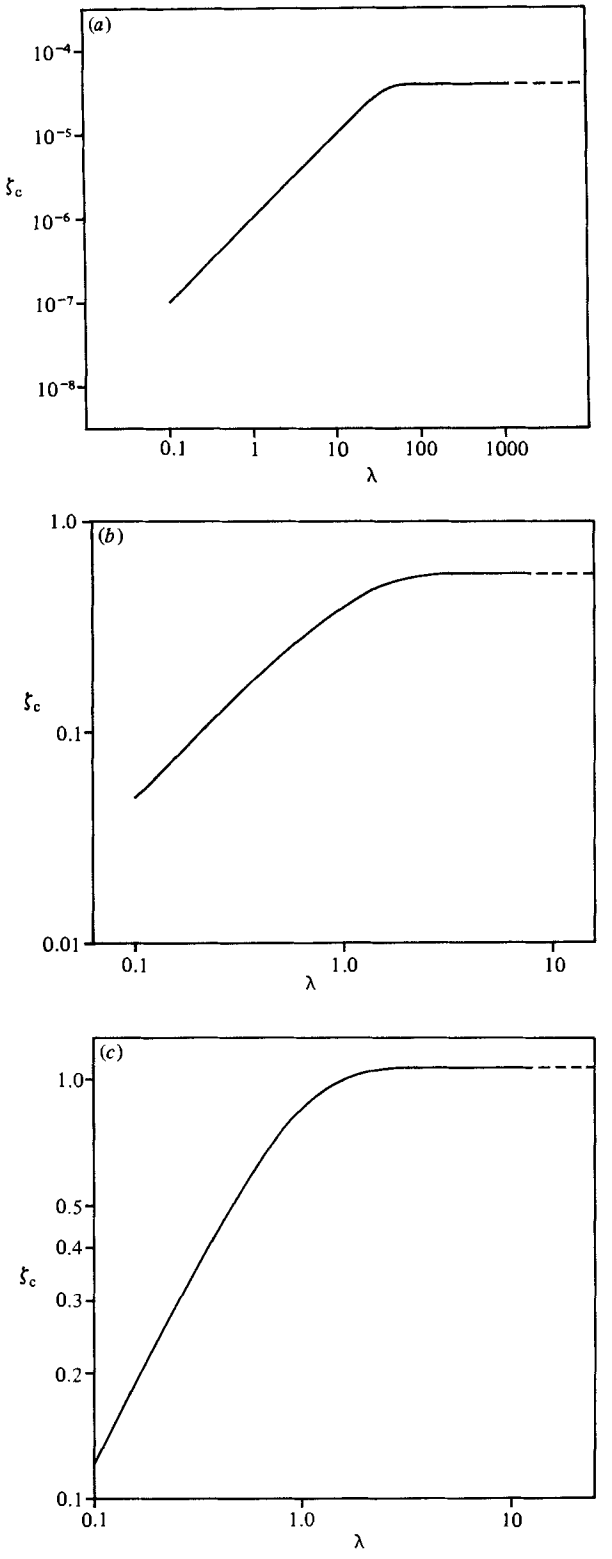

FIGURE 4. Graph of ζ_c as a function of λ for various values of Prandtl number: (*a*) $\sigma = 0.01$; (*b*) 1.0; (*c*) 100. The dashed lines represent the limit $\lambda \to \infty$.

ratio $E^2/F^2 \to 1.5$ as $\zeta \to 0$ for fixed values of σ. The calculations described here also displayed this limiting behaviour, thus providing a useful check on the numerical method.

Figure 3 shows how ζ_c changes with Prandtl number, with $\lambda = 1$. At high values of σ (> 10) the value of ζ_c becomes independent of σ, and appears to approach a value very close to unity. For low-Prandtl-number fluids (e.g. mercury, $\sigma \sim 0.025$) we see from the figure that the value of ζ_c is much less than unity. We find that $\zeta_c \sim \sigma^4$ for small σ, with a constant of proportionality approximately equal to 100.4 (for $\lambda = 1$). It is of interest that the small-ζ theory of Proctor (1981), that predicts square cells for all σ of order unity, breaks down precisely when $\sigma \sim \zeta^{\frac{1}{4}}$; more recent work (Proctor, in preparation) incorporating the effects of small σ in fact gives the same power law with the same constant.

Figure 4 shows the variation of ζ_c with the slab thickness λ for fluids with Prandtl number of 0.01, 1 and 100. In each of these graphs we see that ζ_c becomes independent of λ as λ becomes large. The problem has also been solved for the limit $\lambda \to \infty$ by replacing the boundary condition (2.5) with $\tilde{\theta} \to 0$ as $z \to \infty$ and the limiting value of ζ_c is shown on each of the graphs of figure 4. Also, for small λ we see from the graphs that $\zeta_c = O(\lambda)$, which appears to be the correct behaviour, considering the boundary condition for θ in the linear problem which is

$$\mathrm{D}\theta|_{\pm\frac{1}{2}} = \mp\zeta\alpha \coth(\tfrac{1}{2}\alpha\lambda)\,\theta|_{\pm\frac{1}{2}},$$

and since $\alpha \to 3.117$, as $\lambda \to 0$ for fixed ζ, we see that for small λ this reduces to

$$\mathrm{D}\theta|_{\pm\frac{1}{2}} = \mp 2\zeta/\lambda\,\theta|_{\pm\frac{1}{2}},$$

so that ζ/λ is the only relevant parameter.

6. Discussion

In §5 we have determined the nature of the planform of thermal convection between slabs of finite conductivity for a wide range of values of the Prandtl number σ and slab thickness λ. The results indicate that it may be possible to observe square-cell structures experimentally, but only for fluids with Prandtl number greater than about 1. For instance, consider the experimental work of Whitehead & Chan (1976), which used silicone oil ($\sigma \approx 200$) bounded by glass slabs whose conductivity was approximately 6 times that of the fluid. This type of boundary was required by the experimental apparatus, as transmission of light through the bounding slabs was used to observe the planform. Other transparent boundaries with lower conductivity than glass could be used, and this would reduce the value of ζ to a value less than 1. Should such a situation be feasible, then the above theory predicts that square-cell solutions would be observed at Rayleigh numbers slightly above the critical Rayleigh number R_0, determined by the graph of figure 1. Thus the next step in this study should be an attempt to observe square-cell planforms in laboratory experiments.

It should be noted that λ need not be the same for top and bottom slabs in order to obtain the results presented here, with only quantitative differences in the value of ζ_c being obtained should such an asymmetry occur. The results of Riahi (1983) for the porous problem indicate, however, that if the conductivities k_1 of the top and bottom slabs are sufficiently different, square-cell solutions may not be possible for any ζ.

The authors gratefully acknowledge the advice of D. R. Fearn on numerical problems. One of us (D.R.J.) acknowledges the financial assistance provided under the Commonwealth Scholarships and Fellowships Plan.

REFERENCES

BUSSE, F. H. & RIAHI, N. 1980 Nonlinear convection in a layer with nearly insulating boundaries. *J. Fluid Mech.* **96**, 243–256.

CHAPMAN, C. J. & PROCTOR, M. R. E. 1980 Nonlinear Rayleigh–Bénard convection between poorly conducting boundaries. *J. Fluid Mech.* **101**, 759–782.

HURLE, D. T. J., JAKEMAN, E. & PIKE, E. R. 1967 On the solution of the Bénard problem with boundaries of finite conductivity. *Proc. R. Soc. Lond.* A **296**, 469–475.

JEFFREYS, H. 1926 The stability of a layer heated from below. *Phil. Mag.* **2**, 833–844.

MALKUS, W. V. R. & VERONIS, G. 1958 Finite amplitude cellular convection. *J. Fluid Mech.* **4**, 225–260.

PROCTOR, M. R. E. 1981 Planform selection by finite-amplitude thermal convection between poorly conducting slabs. *J. Fluid Mech.* **113**, 469–485.

RIAHI, N. 1983 Nonlinear convection in a porous layer with finite conductivity boundaries. *J. Fluid Mech.* **129**, 153–171.

SCHLUTER, A., LORTZ, D. & BUSSE, F. 1965 On the stability of steady finite amplitude convection. *J. Fluid Mech.* **23**, 129–144.

SPARROW, E. M., GOLDSTEIN, R. J. & JONSSON, V. H. 1964 Thermal instability in a horizontal fluid layer: effect of boundary conditions and nonlinear temperature profile. *J. Fluid Mech.* **18**, 513–528.

WHITEHEAD, J. A. & CHAN, G. L. 1976 Stability of Rayleigh–Bénard convection rolls and bimodal flow at moderate Prandtl number. *Dyn. Atmos. Oceans* **1**, 33–49.